Tele-operated propeller-type climbing robot for inspection of petrochemical vessels

Mohamed Gouda Alkalla
Department of Mechatronics and Robotics Engineering, Egypt-Japan University of Science and Technology, Alexandria, Egypt and Department of Physics and Applied Physics, Waseda University, Tokyo, Japan
Mohamed A. Fanni
Department of Mechatronics and Robotics Engineering, Egypt-Japan University of Science and Technology, Alexandria, Egypt and Production Engineering and Mechanical Design Department, Faculty of Engineering, Mansoura University, Egypt
Abdelfatah M. Mohamed
Department of Mechatronics and Robotics Engineering, Egypt-Japan University of Science and Technology, Alexandria, Egypt and Department of Electrical and Electronics Engineering, Assiut University, Egypt, and
Shuji Hashimoto
Department of Physics and Applied Physics, Waseda University, Tokyo, Japan

Abstract

Purpose – The purpose of this paper is to propose a new propeller-type climbing robot called EJBot for climbing various types of structures that include significant obstacles, besides inspection of industrial vessels made of various materials, including non-ferromagnetic material. The inspection includes capturing images for important spots and measuring the wall thickness.

Design/methodology/approach – The design mainly consists of two coaxial upturned propellers mounted on a mobile robot with four standard wheels. A new hybrid actuation system that consists of propeller thrust forces and standard wheel torques is considered as the adhesion system for this climbing robot. This system generates the required adhesion force to support the robot on the climbed surfaces. Dynamic simulation using ADAMS is performed and ensures the success of this idea.

Findings – Experimental tests to check the EJBot's capabilities of climbing different surfaces, such as smooth, rough, flat and cylindrical surfaces like the real vessel, are successfully carried out. In addition, the robot stops accurately on the climbed surface at any desired location for inspection purposes, and it overcomes significant obstacles up to 40 mm.

Practical implications – This proposed climbing robot is needed for petrochemical and liquid gas vessels, where a regular inspection of the welds and the wall thickness is required. The interaction between the human and these vessels is dangerous and not healthy due to the harmful environment inside these vessels.

Originality/value – This robot utilizes propeller thrusts and wheel torques simultaneously to generate adhesion and traction forces. Therefore, a versatile robot able to climb different kinds of structures is obtained.

Keywords Inspection, Climbing, Propeller, Vessels

Paper type Research paper

1. Introduction

The importance of climbing robots has risen during the past two decades due to their applications in different civilian and industrial fields, such as rescue purposes, firefighting at high-rise buildings and inspection of bridges, highways, ship hulls, turbines, towers of nuclear power plants and petrochemical industry vessels.

A lot of climbing robots are initially designed and proposed for climbing a specific kind of structure or surface. Some of these robots, called magnetic-adhesion robots, are built to fit the ferromagnetic structures such as tubes, pipes and steel bridges. These robots use magnetic wheels, tracks or legs (Tavakoli *et al.*, 2013; Kalra *et al.*, 2006; Grieco *et al.*, 1998). The advantage of this adhesion type is a strong and stable adhesion force; its drawback is that this kind of adhesion is limited only to the ferromagnetic structure.

Another group of the climbing robots which fits only flat and even surfaces (i.e. flat concrete or glass buildings) are the aerodynamic or air suction adhesion robots. Most of these robots use passive suction cups where the robot can attach and remove its suction cups passively, as presented by Yoshida and Ma (2010) and Lee *et al.* (2015), or active suction chambers with

The current issue and full text archive of this journal is available on Emerald Insight at: **www.emeraldinsight.com/0143-991X.htm**

Industrial Robot: An International Journal
44/2 (2017) 166–177

[DOI 10.1108/IR-07-2016-0182]

The first author gratefully thanks the Cultural Affairs and Missions Sector, Ministry of Higher Education (MoHE), Egypt for funding him with a full doctorate scholarship. The authors are so grateful to Eng. Omar Ibn El Khatab at E-JUST for his valuable contribution in the experimental work and all the department colleagues.

Received 6 July 2016
Revised 2 October 2016
Accepted 25 October 2016

seals to keep a pressure difference between the inside and the outside of these chambers, as presented by Mohamed *et al.* (2014), Hillenbrand *et al.* (2008) and Guan *et al.* (2013). The advantage of air suction adhesion is the ability to climb any material type, not only ferromagnetic surfaces. Its drawbacks are requirement of proximity between the surface and suction chamber, and possible seal damage or vacuum loss due to rough surfaces. Therefore, the robots that use this kind of adhesion would not be able to overcome significant obstacles. Obstacle avoidance and robot localization are also issues. Holes are a critical issue for vacuum-based climbers because these systems lose the mandatory vacuum between the wall and the robot. Other examples of aerodynamic adhesion are LARVA (Koo *et al.*, 2013) and City Climber (Xiao and Sadegh, 2007), which use impellers and vacuum chambers to generate a low-pressure zone enclosed by the chamber. Although the vacuum chamber in this case does not need a physical contact with the surface, it requires a quite proximity for a strong adhesion. Therefore, the maximum size of obstacles that could be overcome is around 10 mm, besides the limitations on climbing cylindrical surfaces or crossing over holes to avoid vacuum loss.

Another group of climbing robots, which are suitable only for the uneven and complex structures, such as, trees, poles and rough building surfaces, are called mechanical adhesion robots. These robots use grippers and claws for grasping the uneven surfaces, as presented in Asbeck and Cutkosky (2012), Guan *et al.* (2016), and Lam and Xu (2011). The advantage of this type of adhesion is the ability to climb irregular and rough surfaces; however, it cannot climb the flat and smooth surfaces. A new kind of climbing robots which recently emerged with the development of materials science are called electrostatic adhesion robots. These robots depend on electrostatic or van der Waals forces between the robot and the surface. Most of these robots are inspired from climbing animals or reptiles, such as the gecko (Menon *et al.*, 2004; Kim *et al.*, 2008). This kind of adhesion system is suitable only for smooth surfaces, including glass, acrylic and plastic panels. More details on the different kinds of climbing robot are presented in Schmidt and Berns (2013).

It is noticed that there is no climbing robot that can handle different surface materials and topologies efficiently. Each climbing robot is suitable only for a narrow range of these varieties. Therefore, a propeller-type climbing robot is mainly proposed here to climb any surface, such as ferromagnetic or non-ferromagnetic and regular or irregular surfaces with significant obstacles. The idea of proposing such a robot comes from the urgent needs of petrochemical and liquefied petroleum gas (LPG) industries to have a versatile climbing robot capable of exploring and climbing the vessels' interiors (Figure 1) considering irregular surfaces/obstacles and the fact that some of these vessels are made of austenitic stainless steel, which does not have a magnetic characteristic. The proposed robot here depends on a hybrid actuation system which utilizes the thrust forces of propellers and the torques of four wheels simultaneously to create the required adhesion force. This adhesion force is needed to support the robot while climbing and navigating any structure. The proposed robot is also characterized by its simple control and stability as compared with other propeller-type climbing robots in Nishi and Miyagi (1993) and Beardsley (2015). The proposed robot, as shown in Figure 2, is able to climb cylindrical surfaces and overcome significant obstacles that would be found inside the vessels.

Figure 1 A vessel of LPG industries

Source: Courtesy of Aweco Indosteel Perkasa Co

This idea of a hybrid actuation system was successfully tested by simulations accomplished previously by Alkalla *et al.* (2015a, 2015b). The simulation results were encouraging enough to carry out experimental works. The beginning of using propellers with climbing robots was in 1990s by Nishi and Miyagi (1991, 1993) and Nishi *et al.* (1995), where the propeller thrust forces were used as the only source of adhesion and navigation. Two inclined propellers were supported on a platform with many passive wheels. This inclined-propeller robot was proposed to climb high-rise buildings for rescue and firefighting purposes. The thrust force is inclined a little to the wall side to produce the frictional force between the wheels and the wall, while the whole weight of the robot is supported by the vertical component of the thrust force. The drawbacks of this robot were its heavy weight and large size, besides the stability of this system was too low, which hindered further research, as reported in Schmidt and Berns (2013). Another propeller-type climbing robot called VertiGo is proposed by the Disney Research Center on their website (Beardsley, 2015). This robot uses two tiltable propellers with passive steerable wheels. The VertiGo robot also depends on the thrust forces that come from these tiltable propellers as the only source for generating the adhesion force, which may cause a problem of stability too, unless a more sophisticated control technique is used. Unlike the previous propeller climbing robots which depend only on the thrust force of the propellers, the proposed robot uses a hybrid actuation system consisting of propeller thrust forces and wheel torques. This adhesion system provides a good and stable adhesion and simple and robust control where the axes of the propellers are fixed and the required thrust forces should be above certain limit. Hence, proper wheel torques can control the robot navigation accurately. The contribution of the motorized wheels in the adhesion system reduces greatly the required thrust forces. Hence, a realistic propeller's size and realistic design come up with a stable and high maneuverable system. This idea identifies the contribution of this work, as will be presented in the next section.

Figure 2 Climbing cylindrical surfaces of huge pipes

(a) **(b)**

Notes: (a) Outer surface of a vertical pipe; (b) inner surface of horizontal pipe

2. The proposed robot design

EJBot consists mainly of three units; the thruster unit, the driving unit and the control unit, as shown in Figure 3. The thruster and driving units should be simultaneously actuated to obtain the adhesion force required to support the robot while climbing the surfaces. The robot is tele-operated by a PS2 wireless control unit to possess flexibility of selecting and checking the critical spots inside the vessels with the aid of a camera and suitable sensors. There are many advantages of this robot. First, contrary to the magnetic adhesion robots, the proposed robot can climb structures made of arbitrary materials. Second, it does not use seals, in contrast to air suction and impeller robots, which have the problem of unreliable sealing when climbing uneven surfaces, facing significant obstacles or crossing over holes. Moreover, the proposed robot saves enough space beneath its frame, which allows it to overcome significant obstacles. Therefore, it can handle obstacles of considerable sizes and navigate over a fairly wide range of surface topologies. Also, the proposed robot can be held still at an arbitrary position to carry out the inspection task using simple control, in contrast to other propeller-type climbing robots. The robot design utilizes two coaxial upturned propellers (right- and left-handed) turning in opposite directions to cancel the drag moments, in addition to four standard actuated wheels, as shown in Figure 4. The right wheels are driven by one motor and so are the left wheels. Two timing belts are used to transmit the torques between the rear and front wheels. This arrangement maximizes the tractive forces between the wheels and the climbed surface and keeps the robot weight minimum rather than using a motor on each wheel. The advantages of this design include a simple mathematical model, where there is no drag moment exerted on the frame, and the compactness in the radial direction, where the two propellers are coaxially mounted on the robot. The mechanical design is carried out with the aid of 3D modeling software (Solid Edge ST6). The static analysis is performed to check the capabilities of the robot for climbing and holding still on a wall at an arbitrary inclination angle. The propeller thrust forces, robot weight, wheel torques and the coefficient of friction between the wheel tires and the climbed surface are taken into consideration. It is important to determine the required propeller thrust forces and the wheel torques at an equilibrium state where the robot stops or moves with constant speed on the climbed surface. Then, these

Figure 3 The main units of the propeller-type climbing robot

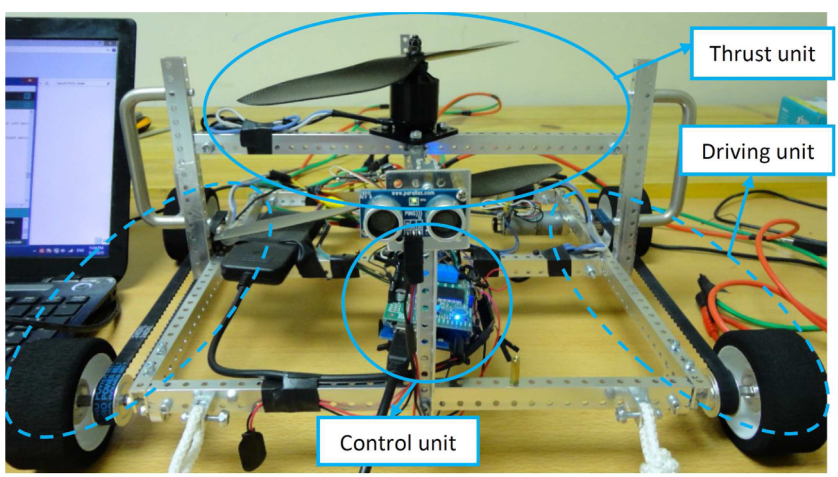

Figure 4 CAD model of the proposed climbing robot

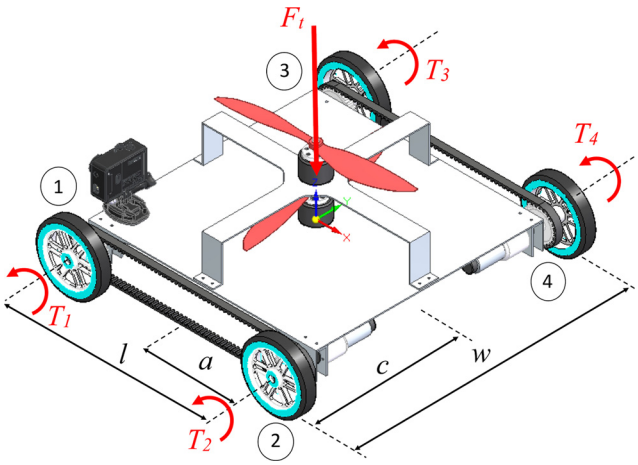

forces and torques can be controlled to satisfy the required climbing scenarios.

All forces and torques acting on the robot frame and wheels are included in the free body diagram, as shown in Figure 5. The equations which hold the robot on a wall with an inclination angle ϕ are derived below:

$$\sum F_x: \quad \sum_{i=1}^{4} F_{ri} - W\cos\phi - F_t = 0 \tag{1}$$

$$\sum F_y: \quad \sum_{i=1}^{4} F_{fi} - W\sin\phi = 0 \tag{2}$$

where F_t is the resultant propellers' thrust force; F_{ri} and F_{fi} are normal reaction force and frictional force on wheel i, respectively; and W is the robot weight. The moments about x, y and z-axes which are passing through the center of mass (COM) are used to get the relationship between the design parameters and forces, as follows:

Figure 5 Free body diagram of the action and reaction forces on the robot

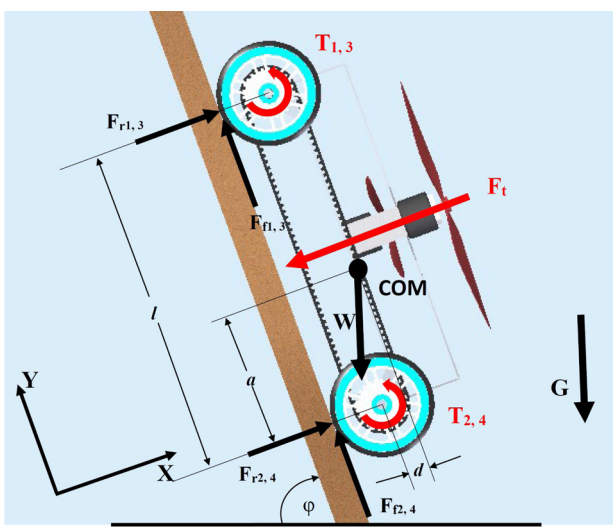

$$\sum M_x: \quad c\left(-\sum_{i=1}^{2} F_{fi} + \sum_{i=3}^{4} F_{fi}\right) = 0 \tag{3}$$

$$\sum M_y: \quad c\left(\sum_{i=1}^{2} F_{ri} - \sum_{i=3}^{4} F_{ri}\right) = 0 \tag{4}$$

$$\sum M_z: \quad F_t\left(\frac{l}{2} - a\right) - \sum_{i=1}^{4} F_{fi}(d + r) - \sum_{i=1,3} F_{ri}(l - a) + \sum_{i=2,4} F_{ri}\, a = 0 \tag{5}$$

where l is the longitudinal distance between the front and rear wheel axles, c is the lateral distance between COM and the wheels, a is the longitudinal distance between COM and the rear wheels' axis, d is the orthogonal distance between COM and the plane which includes the four wheels' axes and r is the wheel radius. The relationship between the wheel torques, T_i, and the frictional forces for non-slippage condition is defined as:

$$T_i = F_{fi}\, r \qquad for \quad i = 1, \ldots, 4 \tag{6}$$

There are some propositions for this analysis can be stated as follows:

1 assume non slip condition in longitudinal direction of wheels;
2 the equilibrium condition is considered; and
3 the wheels have the same size and material.

Under these propositions and with utilization of timing belts, the torques and the frictional forces of the front and rear wheels at each side are equal; therefore, $F_{f1} = F_{f2}$ and $F_{f3} = F_{f4}$. For a certain thrust force, robot weight and geometry, there are six unknowns (F_{r1}, F_{r2}, F_{r3}, F_{r4}, F_{f1} and F_{f3}), while we have five equations (1)-(5). Hence, the model is statically indeterminate. The force displacement method is used for compatibility, considering the robot frame as a rigid body and its wheels as flexible bodies, as shown in Figure 6. Therefore, a relationship between the displacements of the wheels is obtained using the equation of a plane. This displacement equation is transformed to a relationship in the reaction forces. Thus, the last equation to solve the system is derived as follows:

$$\sum_{i=1,4} \frac{F_{ri}}{k_i} - \sum_{i=2,3} \frac{F_{ri}}{k_i} = 0 \tag{7}$$

where k_i is the stiffness of wheel i. In the case of using similar wheels, k_i can be omitted from equation (7). The robot can be held in its place or moved with a constant velocity if the frictional force is less than the reaction force multiplied by the sliding static coefficient of friction, μ_s, at each wheel, as expressed in equation (8). This equation determines the capacity of the traction forces of the wheels and provides an essential check to validate the robot design.

$$F_{fi} \le \mu_s\, F_{ri} \qquad for \quad i = 1, \ldots, 4 \tag{8}$$

Figure 6 Force-displacement method for the robot frame

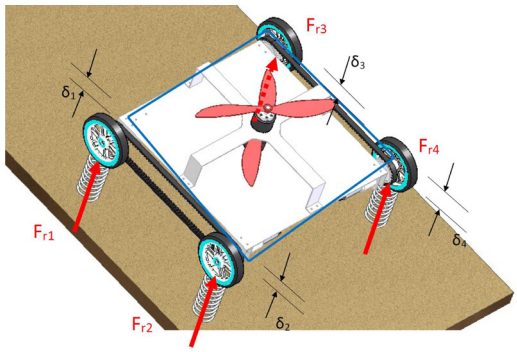

This system of equations can be written in this form:

$$AX = B \tag{9}$$

where,

$$X = [F_{r1} \;\; F_{r2} \;\; F_{r3} \;\; F_{r4} \;\; F_{f1} \;\; F_{f2} \;\; F_{f3} \;\; F_{f4}]^T, \tag{10}$$

$$A = \begin{bmatrix} 1 & 1 & 1 & 1 & 0 & 0 & 0 & 0 \\ 0 & 0 & 0 & 0 & 1 & 1 & 1 & 1 \\ 0 & 0 & 0 & 0 & -c & -c & c & c \\ c & c & -c & -c & 0 & 0 & 0 & 0 \\ -(l-a) & a & -(l-a) & a & -(d+r) & -(d+r) & -(d+r) & -(d+r) \\ 0 & 0 & 0 & 0 & 1 & -1 & 0 & 0 \\ 0 & 0 & 0 & 0 & 0 & 0 & 1 & -1 \\ 1/k_1 & -1/k_2 & -1/k_3 & 1/k_4 & 0 & 0 & 0 & 0 \end{bmatrix}, \tag{11}$$

$$B = \left[W\cos\phi + F_t \;\; W\sin\phi \;\; 0 \;\; 0 \;\; -F_t\left(\frac{l}{2} - a\right) \;\; 0 \;\; 0 \;\; 0 \right]^T \tag{12}$$

The robot weight approximately equals 1.66 kg, and the maximum thrust force for the propellers is 5 kgf. All the specifications of the robot are given in Table I. To check the robot's adhesion capacity, including the normal and frictional forces on each wheel, curves are plotted between these forces and the surface inclination angle (ϕ), which varies from 0° to 360°. The safe zone of the wheel traction forces is obtained from these plots. Consequently, one can check/estimate the required torques of the wheels' motors that satisfy the non-slippage condition in equation (8). The normal reaction forces on the front and rear wheels versus the inclination angle are shown in Figure 7. These normal forces should be greater than zero to ensure the contact between the robot wheels and the climbed surface. The required frictional forces on the front and rear wheels to keep the robot in static equilibrium state on a wall, considering all design parameters in Table I, are shown in Figure 8 (black curve). It shows that the maximum absolute frictional forces are required at the vertical position at $\phi = 90^o$ (ascent) and $\phi = 270^o$ (descent). This figure also illustrates the maximum allowed frictional force or the traction forces' capacity for the front and rear wheels presented by red and blue curves, respectively. This maximum allowed frictional force is calculated from equation (8) by multiplying the coefficient of friction by the wheel normal forces. Therefore, the capacity of traction forces is located between the red or blue curve and the zero line for the front or rear wheels, respectively. This region can be called the non-slippage zone for the wheels' actuation. The forces acting on the robot while climbing a cylindrical surface in the circumferential path can be presented. This analysis is important to get a more accurate force analysis in case of

Table I The climbing robot (EJBot) specifications

Properties	Value
Length between wheel centers (*l*)	303.29 mm
Whole robot length	350 mm
Width (*w*)	350 mm
Center of mass (*a*)	145 mm
Thickness (*t*)	2 mm
Propeller diameter (D_p)	12 inch
Weight (*W*)	1,660 g
Frame density (ρ)	2,700 kg/m^3
Thrust force (F_t)	5 kgf
Coefficient of friction (μ_s)	0.4
Wheel radius (*r*)	50 mm
Orthogonal distance (*d*)	15 mm
Max. torque of wheel motors (T_{max})	1400 N.mm

Figure 7 Normal reaction forces on the front and rear wheels versus inclination angle

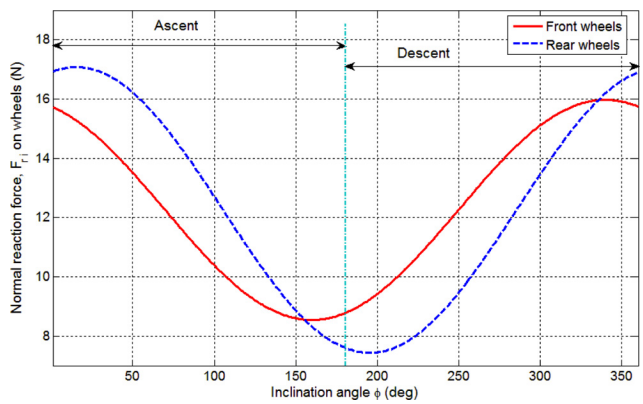

Figure 8 Required frictional forces and their maximum capacity on the wheels versus inclination angle

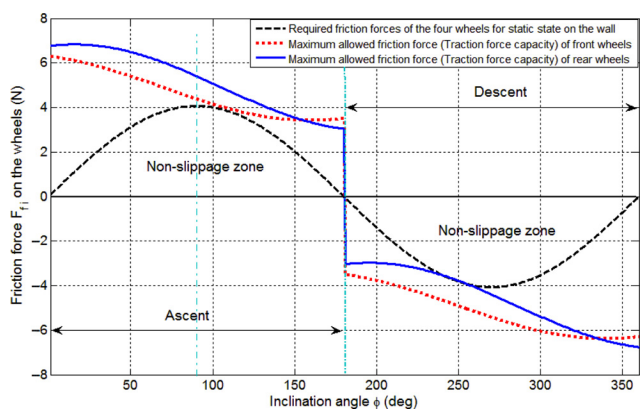

climbing any cylindrical surface of the vessels with radius R, as shown in Figure 9. The force analysis is applied considering an inclination angle ϕ between the cylinder fixed coordinates (X, Y) and the robot coordinates (X_r, Y_r). Hence, the static equations can be derived with respect to the robot coordinates as follows:

$$\sum F_x: -(F_{r2} + F_{r4})\sin\delta_1 + (F_{r1} + F_{r3})\sin\delta_2 - (F_{f2} + F_{f4})\cos\delta_1 - (F_{f1} + F_{f3})\cos\delta_2 - F_t\sin\delta_3 + W\sin\phi = 0 \quad (13)$$

$$\sum F_y: (F_{r2} + F_{r4})\cos\delta_1 + (F_{r1} + F_{r3})\cos\delta_2 - (F_{f2} + F_{f4})\sin\delta_1 + (F_{f1} + F_{f3})\sin\delta_2 - F_t\cos\delta_3 - W\cos\phi = 0 \quad (14)$$

$$\sum M_x: c[(F_{r3} - F_{r1})\cos\delta_2 + (F_{f3} - F_{f1})\sin\delta_2 + (F_{r4} - F_{r2})\cos\delta_1 - (F_{f4} - F_{f2})\sin\delta_1] = 0 \quad (15)$$

$$\sum M_y: c[-(F_{r3} - F_{r1})\sin\delta_2 + (F_{f3} - F_{f1})\cos\delta_2 + (F_{r4} - F_{r2})\sin\delta_1 + (F_{f4} - F_{f2})\cos\delta_1] = 0 \quad (16)$$

$$\sum M_z: -b[(F_{r1} + F_{r3})\cos\delta_2 + (F_{f1} + F_{f3})\sin\delta_2] + a[(F_{r2} + F_{r4})\cos\delta_1 - (F_{f2} + F_{f4})\sin\delta_1] + \left(\frac{l}{2} - a\right)$$

$$F_t\cos\delta_3 + h[(F_{r1} + F_{r3})\sin\delta_2 - (F_{f1} + F_{f3})\cos\delta_2 - (F_{r2} + F_{r4})\sin\delta_1 - (F_{f2} + F_{f4})\cos\delta_1] = 0 \quad (17)$$

The relationship between the wheel torques and the frictional or traction forces is the same as in equation (6), and from the design consideration of using timing belts, the torques of the rear and front wheels at each side are equal, then $F_{f1} = F_{f2}$ and $F_{f3} = F_{f4}$. The complementary equation (7) can be modified to this form:

Figure 9 The force analysis of the robot on a cylindrical surface

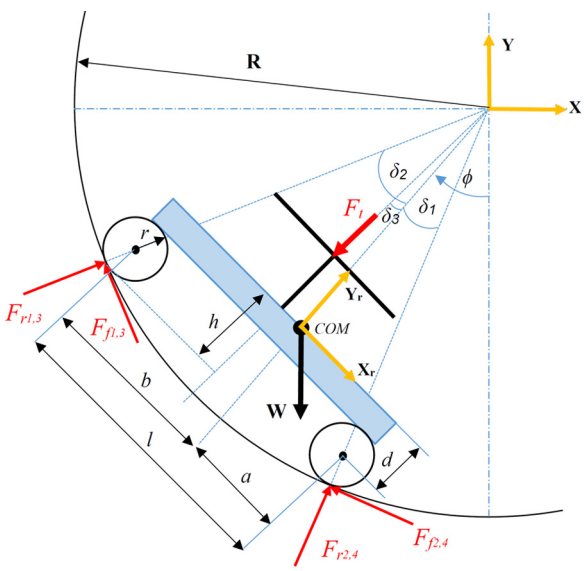

$$\left(\frac{F_{r1}}{k_1} - \frac{F_{r3}}{k_3}\right)\cos\delta_2 - \left(\frac{F_{r2}}{k_2} - \frac{F_{r4}}{k_4}\right)\cos\delta_1 = 0 \quad (18)$$

where b is the distance between the front wheel axes and COM, h is the orthogonal distance between COM and the contact point of wheels with the curved surface ($h \approx d + r$) and the angles δ_1, δ_2 and δ_3 are defined as:

$$\delta_1 \approx \left(\frac{a}{R}\right), \quad \delta_2 \approx \left(\frac{b}{R}\right), \quad \delta_3 \approx \left(\frac{l - 2a}{2R}\right) \quad (19)$$

The required and maximum traction forces and torques for a flat and cylindrical surface with a 5 m diameter are illustrated in Table II. These values are obtained at the worst case of climbing at $\phi = 90°$. They show that the required traction forces and wheel torques for climbing the cylindrical surface are less than those for climbing the flat surface. This because the normal and friction forces in the cylindrical surface model are inclined a little and not in the horizontal and vertical directions, as the case of a flat vertical surface.

It is noted that the robot system needs a simple control to adjust the angular velocities of the wheels as well as to produce nearly constant angular velocities of the propellers and hence get a nearly constant thrust force. The tolerance allowed in the control of the propellers comes from the fact that the thrust force needs to be larger than a certain limit to ensure a non-slipping condition. This is contrary to the previous propeller-type climbing robots (Nishi and Miyagi, 1993; Beardsley, 2015), where the thrust force needs to be equal to a certain value that changes with time to accomplish the navigation and inspection tasks. In the proposed robot, the navigation is done using the motorized wheels rather than the propellers, which ensures stability of the system using a simple control.

3. Dynamic simulation using ADAMS

A dynamic simulation of the robot using ADAMS software is carried out to check the system's capability of climbing vertical and cylindrical surfaces as well as stopping on the surface at a desired location. ADAMS contact facility is used to model the contact between the robot's wheels and the climbed surface. The parameters of the contact are defined as follows. The static and dynamic coefficients of friction are equal to 0.4 and 0.3, respectively; the stiffness of the wheels is 10^4 N/mm; the damping coefficient is 10^4 N.s/mm; and penetration depth is 0.1 mm. In addition, the stiction and the friction transition velocity are 1 mm/s and 100 mm/s, respectively. All the design parameters, thrust forces and required wheel torques which are determined in the previous section in Tables I and II are included in this simulation. The first simulation is performed to climb the vertical surface. The thrust force of 5 kgf and wheel torque of 203.47 at $\phi = 90°$ (in Table II) are used. The simulation shows that the robot stops at its position on the wall at this actuation torque. When the wheel torques increase a little bit to become 205 N.mm, the robot begins to climb the wall, as shown in Figure 10.

The second simulation is performed to check the robot's ability to climb the inner cylindrical surface of a vessel with 5 m diameter. The simulation test is carried out to make the robot climb inside the vessel in a circumferential path. The

Table II Required and maximum allowed traction forces and wheel torques for flat and cylindrical surfaces at $\phi = 90^{o}$

Forces and torques	Flat surface	Cylindrical surface
Required frictional force on each wheel, F_{fi}	4.069 N	3.958 N
Required actuation torque for each wheel, T_i	203.47 N.mm	197.87 N.mm
Maximum allowed traction forces of front wheels, $F_{f1,3(max)}$	4.298 N	4.204 N
Maximum allowed traction forces of rear wheels, $F_{f2,4(max)}$	5.507 N	5.586 N
Maximum allowed torque of front wheels, $T_{1,3(max)}$	214.92 N.mm	210.21 N.mm
Maximum allowed torque of rear wheels, $T_{2,4(max)}$	275.38 N.mm	279.33 N.mm

Figure 10 Position and velocity of the robot while climbing a vertical surface, simulation by ADAMS

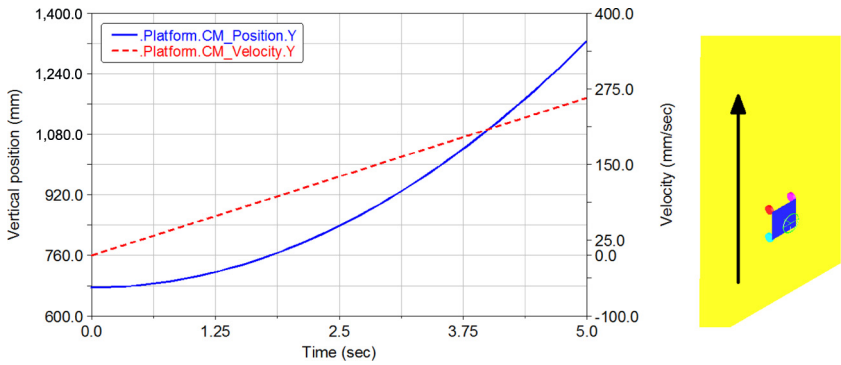

robot begins its motion from the vessel's bottom and climbs until it reaches the top and returns again to the bottom (Figure 11). The actuation torque of 197.87 N.mm at $\phi = 90^{\circ}$ (in Table II) and the same thrust force are used. It is noticed that this torque can be decreased to 180 N.mm and the robot can still climb the inner surface of the vessel. This may be due to the momentum that the robot gains from the beginning of motion at the bottom. The position in horizontal and vertical directions as well as the velocity magnitude of the robot are shown in Figure 12. It is noticed from Figures 10 and 12 that the robot has undesirably increasing speed, where there are no limitations on the wheel speed. PI control with weight compensation was proposed previously by Alkalla *et al.* (2015a) to get a moderate and constant speed for the climbing robot, and hence, facilitating the inspection processes. The wheel torques which represent the input signals of the system are limited to be within the allowed motors' torque capacity.

The simulation results show the validity of the force analysis in the previous section and the idea of climbing using such a hybrid actuation system. The experimental work is presented in the next section, where different climbing scenarios are performed to check the robot capabilities.

Figure 11 Simulation of the robot inside a vessel by MSC ADAMS software

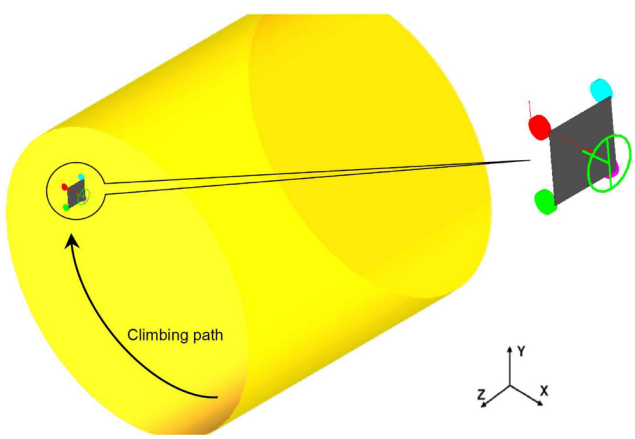

4. Experimental results

The robot frame is built up of aluminum-6061 beams with U-shaped cross-section to be light and stiff. The robot components are classified as follows: two DC brushless motors, each having a power of 380 W, two carbon fiber propellers of 12 inch diameter, four wheels made of a compound foam with a high coefficient of friction and two 12-V geared motors mounted on the rear wheels. The source of power is two lithium polymer (LiPo) batteries, each one has three cells with 11.1 V and 8,400 mAh. The batteries are connected in series and generate a high current that the brushless motors need. Each brushless motor requires a maximum current of 20 A to generate a thrust force of 2.5 kgf. The control unit consists mainly of Arduino mega-2560 board, two electronic speed controllers (ESC) as drivers for the brushless motors, a dual-motor driver shield for the two DC-geared motors and a PS2 receiver and transmitter. The PS2 receiver is attached directly to the Arduino board, while the robot operator can hold the PS2 transmitter and keep some distance from the inspection area for safety considerations. The sensors attached to the robot are an ultrasonic sensor for measuring the distance and wheel motor encoders for measuring the wheel number of rotations. A schematic diagram representing the electrical power and signal flow between the different control units is shown in Figure 13.

Figure 12 The position and velocity of the robot inside the vessel

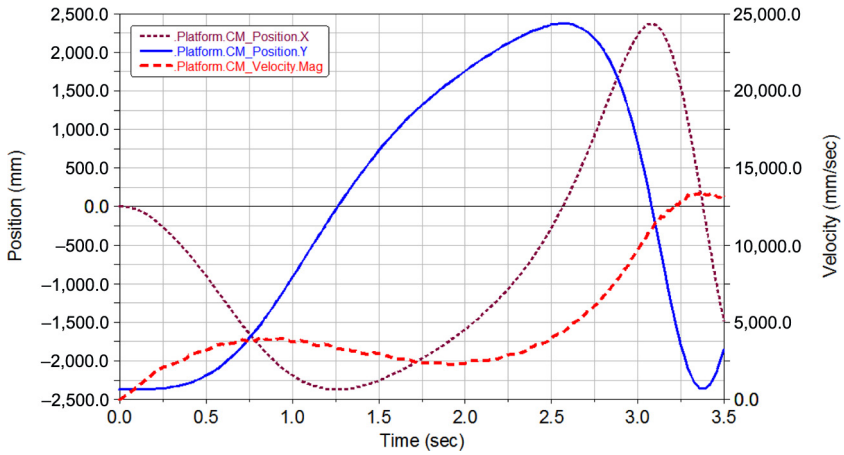

Figure 13 Schematic diagram for the power and signal flow between the robot components

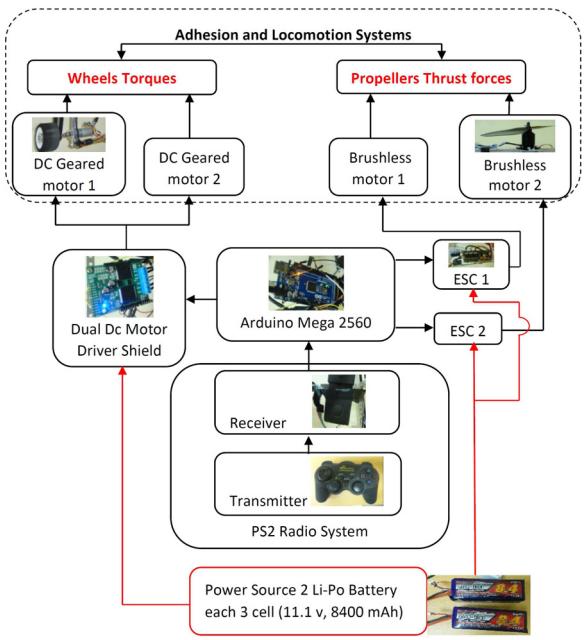

The weight of the two batteries is nearly 1.2 kg, so it is difficult to mount them on the robot platform due to their heavy weight. Hence, it is better to connect them by an umbilical cord.

There are different experimental tests carried out to check the robot's capability of climbing various surfaces with different climbing scenarios. The first test is performed to climb a vertical wall in the laboratory, as shown in Figure 14. However, the wall surface is very smooth; this test shows that the robot has the ability to climb such surfaces. An odometry method for detecting the robot position during climbing is used, where the encoders are used to provide the number of revolutions of the wheels, and hence, they can be interpreted to a traveling distance. Although this odometry method can predict the robot position, it does not give an accurate position of the robot due to the wheel slippage. Consequently, a

Figure 14 Climbing a smooth wall in the laboratory

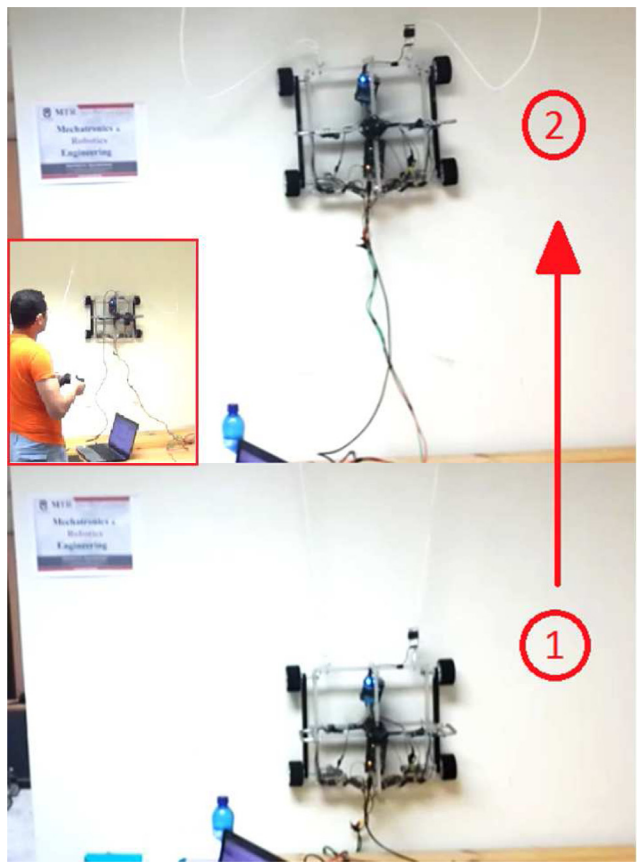

ground truth way should be obtained to get the real position based on the fixed or ground frame. The ultrasonic sensor is used here to measure the vertical position of the robot with respect to its initial position. The readings of the ultrasonic sensor are filtered by a low-pass filter and plotted in Figure 15 in addition to the encoder readings. The figure shows the vertical position of the robot measured by the wheel encoders and the ultrasonic sensor and obviously displays the slippage that occurs between the wheels and the wall. These results emphasize the importance of using range sensors in addition

Figure 15 Slippage detection by comparing the encoders and ultrasonic readings

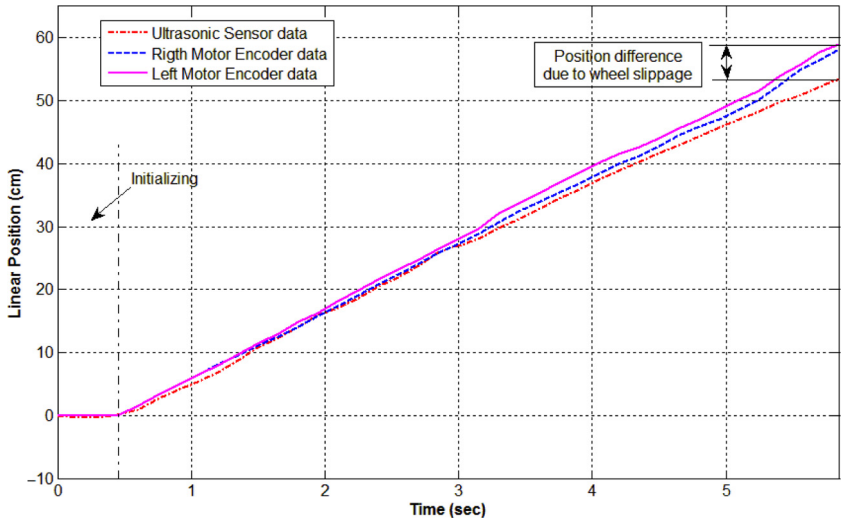

to odometry to successfully control the robot position if it works autonomously. However, the current robot is teleoperated to inspect industrial vessels. The robot can easily overcome significant obstacles where there is no physical contact between the robot platform and the wall. The obstacle sizes that the robot can overcome are up to 40 mm. This value is sufficient for the robot to overcome welding lines or any protrusion on the surfaces (i.e. bolt heads, nuts, etc.). This height can also be increased where it is proportional to the wheel radius. The robot is also tested to move in a horizontal direction on the wall and on the ceiling, as shown in Figures 16 and 17, respectively.

The next experiments are accomplished outdoors for climbing a huge concrete pipe with a diameter of 3 m. This test imitates climbing the cylindrical surfaces of real industrial vessels. The robot proves its success in climbing the outer surfaces of the pipe, as shown previously in Figure 2(a), and the inner surface of the pipe in a circumferential path, as shown in Figure 18. The average speed of the robot in the experimental tests is nearly 250 mm/s. Table III shows the robot speed at different climbing tasks according to the measured distance and time. The payload capacity of the robot is 600 g, as shown in Figure 19. This value is enough for carrying a wireless camera with lighting system, such as "TTL Serial JPEG Camera with NTSC Video and IR LEDs", where its weight is 150 g only. The targeted inspection tasks of the robot are considered as non-destructive tests, such as a visual inspection of the weld lines and corrosion inside the inaccessible vessels (Figure 20). All the data and images of these critical spots should be captured and sent outside the vessels to the inspection team. Wall thickness measurement is also an essential task which uses basically ultrasonic tools. The ultrasonic sensor can be mounted on the climbing robot and scans the surface by moving the robot in a defined pattern. The thickness of the surface can be detected by measuring the traveling time of the ultrasonic waves inside the surface. A wall thickness sensor, e.g. DM5E, weighs only about 200 g. Therefore, the robot can handle this sensor easily. More details on the vessels inspection are presented in van den Bos *et al.* (2015).

5. Conclusions

This article presents a new propeller-type climbing robot called EJBot which uses a hybrid actuation system consisting of propeller thrust forces and wheel torques. The success and stability of this hybrid system are proved by both the dynamic simulation and the experimental tests. The robot is efficiently tele-operated by a PS2 radio control unit. The experimental results show the robot's ability of climbing, exploring and

Figure 16 Climbing the wall and moving in a horizontal direction

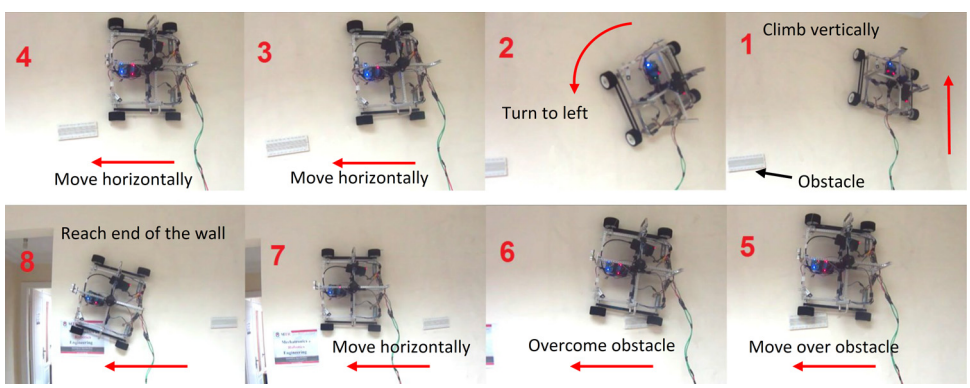

Figure 17 Moving on the ceiling and top of curved surface

(a) **(b)**

Notes: (a) Ceiling of the laboratory; (b) top of curved surface

Figure 18 Climbing the inner surface of a huge concrete pipe

Table III The robot speed in different climbing tests

Velocity	Vertical motion	Horizontal motion	Ceiling	Curved surface/ pipe interior
Linear velocity	140 mm/s	300 mm/s	250 mm/s	260 mm/s

Figure 19 EJBot is climbing a curved surface and carrying 600-g payload

Figure 20 Weld corrosion inside a liquefied natural gas vessel

Source: LNG Idku Co., Egypt

moving in arbitrary directions on a vertical structure and on the ceiling, as well as climbing inner and outer cylindrical surfaces. This robot outperforms many climbing robots in some aspects, such as its ability to climb different types of surface materials and topologies as well as its small size and weight. It also has a good maneuverability, sufficient stability, simple control and capability of overcoming significant obstacles. The average robot speed during different experimental tests ranges from 140 to 300 mm/s and the payload capacity is 600 g. The recommendations for the future work will be to use a more powerful LiPo battery with minimum weight to be mounted directly on the robot without using the umbilical cord, and to implement a transition mechanism for climbing orthogonal surfaces, such as the transition from ground to wall or wall to ceiling.

References

Alkalla, M., Fanni, M. and Mohamed, A. (2015a), "A novel propeller-type climbing robot for vessels inspection", *2015 IEEE International Conference on Advanced Intelligent Mechatronics (AIM)*, pp. 1623-1628.

Alkalla, M.G., Fanni, M.A. and Mohamed, A.F. (2015b), "Versatile climbing robot for vessels inspection", *2015 International Conference on Control, Automation and Robotics (ICCAR)*, pp. 18-23.

Asbeck, A.T. and Cutkosky, M.R. (2012), "Designing compliant spine mechanisms for climbing", *Journal of Mechanisms and Robotics*, Vol. 4 No. 3.

Beardsley, P. (2015), "VertiGo a wall-climbing robot including ground-wall transition", available at: www.disneyresearch.com/publication/vertigo/ (accessed 29 December 2015).

Grieco, J.C., Prieto, M., Armada, M. and de Santos, P.G. (1998), "A six-legged climbing robot for high payloads", *Proceedings of the 1998 IEEE International Conference on Control Applications*, pp. 446-450.

Guan, Y., Zhu, H., Wu, W., Zhou, X., Jiang, L., Cai, C., Zhang, L. and Zhang, H. (2013), "A modular biped wall-climbing robot with high mobility and manipulating function", *IEEE/ASME Transactions on Mechatronics*, Vol. 18 No. 6, pp. 1787-1798.

Guan, Y., Jiang, L., Zhu, H., Wu, W., Zhou, X., Zhang, H. and Zhang, X. (2016), "Climbot: a bio-inspired modular biped climbing robot system development, climbing gaits, and experiments", *Journal of Mechanisms and Robotics*, Vol. 8 No. 2.

Hillenbrand, C., Schmidt, D. and Berns, K. (2008), "Cromsci: development of a climbing robot with negative pressure adhesion for inspections", *Industrial Robot: An International Journal*, Vol. 35 No. 3, pp. 228-237.

Kalra, L.P., Gu, J. and Meng, M. (2006), "A wall climbing robot for oil tank inspection", *IEEE International Conference on Robotics and Biomimetics*, pp. 1523-1528.

Kim, S., Spenko, M., Trujillo, S., Heyneman, B., Santos, D. and Cutkosky, M.R. (2008), "Smooth vertical surface climbing with directional adhesion", *IEEE Transactions on Robotics*, Vol. 24 No. 1, pp. 65-74.

Koo, I.M., Trong, T.D., Lee, Y.H., Moon, H., Koo, J., Park, S.K. and Choi, H.R. (2013), "Development of wall climbing robot system by using impeller type adhesion mechanism", *Journal of Intelligent & Robotic Systems*, Vol. 72 No. 1, pp. 57-72.

Lam, T.L. and Xu, Y. (2011), "Climbing strategy for a flexible tree climbing robot–treebot", *IEEE Transactions on Robotics*, Vol. 27 No. 6, pp. 1107-1117.

Lee, G., Kim, H., Seo, K., Kim, J. and Kim, H.S. (2015), "Multitrack: a multi-linked track robot with suction adhesion for climbing and transition", *Robotics and Autonomous Systems*, Vol. 72, pp. 207-216.

Menon, C., Murphy, M. and Sitti, M. (2004), "Gecko inspired surface climbing robots", *IEEE International Conference on Robotics and Biomimetic*, pp. 431-436.

Mohamed, A.M., Zyada, Z.A. and El-Shenawy, E.A. (2014), "Design, modeling and control of a wall climbing robot crossing over obstacles", *2014 IEEE/SICE International Symposium on System Integration (SII)*, pp. 46-51.

Nishi, A. and Miyagi, H. (1991), "Control of a wall-climbing robot using propulsive force of propeller", *Proceedings of IROS'91. IEEE/RSJ International Workshop on Intelligent Robots and Systems, '91 'Intelligence for Mechanical Systems*, pp. 1561-1567.

Nishi, A. and Miyagi, H. (1993), "Propeller type wall-climbing robot for inspection use", *Proceedings of 10th International Symposium on Automation and Robotics in Construction (ISARC)*, pp. 189-196.

Nishi, A., Miyagi, H. and Ishihara, K. (1995), "Development of wall inspection robots", *Proceedings of 12th International Symposium on Automation and Robotics in Construction (ISARC)*, pp. 103-108.

Schmidt, D. and Berns, K. (2013), "Climbing robots for maintenance and inspections of vertical structures–a survey of design aspects and technologies", *Robotics and Autonomous Systems*, Vol. 61 No. 12, pp. 1288-1305.

Tavakoli, M., Viegas, C., Marques, L., Pires, J.N. and de Almeida, A.T. (2013), "Omniclimbers: omni-directional magnetic wheeled climbing robots for inspection of ferromagnetic structures", *Robotics and Autonomous Systems*, Vol. 61 No. 9, pp. 997-1007.

van den Bos, B., Strand, J., Mallion, A., Oetiker, M., Schler, A., Black, T. and Potnis, P. (2015), "Robotic inspection solutions for petrochemical pressure vessels", *Society of Petroleum Engineers*, doi: 10.2118/177913-MS.

Xiao, J. and Sadegh, A. (2007), "City-climber: a new generation wall-climbing robots", in Zhang, H. (Ed.), *Climbing and Walking Robots: Towards New Applications*, Itech Education and Publishing, Vienna.

Yoshida, Y. and Ma, S. (2010), "Design of a wall-climbing robot with passive suction cups", *2010 IEEE International Conference on Robotics and Biomimetic (ROBIO)*, pp. 1513-1518.

About the authors

Mohamed Gouda Alkalla has received BE and MSc degrees in mechanical design engineering from Production Engineering and Mechanical Design Department, Faculty of Engineering, Mansoura University, Egypt, in 2007 and 2013, respectively. He is a PhD Student at Mechatronics and Robotics Engineering Department, School of Innovative Engineering Design, Egypt-Japan University of Science and Technology (E-JUST), Alexandria, Egypt, and and he is currently visiting research fellow at SHALAB Laboratory, Department of Applied Physics, Waseda University, Tokyo, Japan. His major research

interests include robotics engineering, mechanical design and structural optimization. His recent publications focused on climbing robots and topology optimization. He is a member of ASME, IEEE and IEEE/RAS Robotics and Automation Society. Mohamed Gouda Alkalla is the corresponding author and can be contacted at: mohamed.gouda@ejust.edu.eg

Mohamed A. Fanni received BE and MSc degrees in mechanical engineering from the Faculty of Engineering of both Cairo University and Mansoura University, Egypt, in 1981 and 1986, respectively, and PhD degree in engineering from Karlsruhe University, Germany, in 1993. He is an Associate Professor with Innovation, Graduate School of Engineering Science, Egypt-Japan University of Science and Technology E-JUST, Alexandria; on leave from Production Engineering and Mechanical Design Department, Faculty of Engineering, Mansoura University, Egypt. His major research interests include robotics engineering, automatic control and mechanical design. His current research focuses on design and control of mechatronic systems, surgical manipulators, teleoperation systems and flying/walking robots. Mohamed A. Fanni can be contacted at: mohamed.fanni@ejust.edu.eg

Abdelfatah M. Mohamed received PhD degree from the University of Maryland, College Park, USA, in 1990. Since 1990, he has been an Assistant Professor at the Department of Electrical Engineering, Assiut University. He became an Associate Professor in 1995 and Professor in 2000. From September 1990 to August 1993, he has been a Postdoctoral Fellow at the Department of Mechanical Engineering, University of Texas, Austin, USA. From April 1996 to April 1997, he has been a visiting Professor at the Department of Electrical Engineering, Kanazawa University, Japan. From September 2010 to March 2012, he has been the Head of the Department of Electrical Engineering, Assiut University, Egypt. From April 2012 to September 2013, he has been the Dean of the Faculty of Engineering, Assiut University, Egypt. Currently, he is the Head of the Department of Mechatronics and Robotics Engineering, Egypt-Japan University of Science and Technology. His research interests lie in Robust and intelligent control of magnetic bearing, magnetic levitation systems, robotics, industrial drives and power systems. He is a senior IEEE member. Google Scholar h-index = 10. Abdelfatah M. Mohamed can be contacted at: abdelfatah.mohamed@ejust.edu.eg

Shuji Hashimoto, DEng (Member, IEEE), received BS, MS and DEng degrees in Applied Physics from Waseda University, Tokyo, Japan, in 1970, 1973 and 1977, respectively. He is currently a Professor in the Department of Applied Physics, School of Science and Engineering, Waseda University. Since 2000, he has been a Director of the Humanoid Robotics Institute, Waseda University. From 1979 to 1991, he was with the Faculty of Science, Toho University, Funabashi. He was a Vice President of International Computer Music Association until 2001. He is the author of over 200 technical publications, proceedings, editorials and books. He is a reviewer for many journals and conferences on computer music, computer vision, robotics and neural computing. His research interests are in human communication and Kansei information processing, including image processing, music systems, neural computing and humanoid robotics. From 2003, he serves as Chair of the promotion committee, IEEE Tokyo Section. Membership of professional institutions: IEEE, ICMA (International Computer Music Association), IEICE (Institute of Electronics, Information and Communication Engineers), IPSJ (Information Processing Society of Japan), SICE (The Society of Instrument and Control Engineers), ISCIE, I.I.E.E.J (Institute of Image Electronics Engineers of Japan), RSJ (The Robotics Society of Japan), Human Interface Society of Japan and Virtual Reality Society of Japan. Shuji Hashimoto can be contacted at: shuji@waseda.jp